Primordial black holes and gravitational waves from nonminimally coupled supergravity inflation

Shinsuke Kawai[1,*] and Jinsu Kim[2,3,†]

[1]*Department of Physics, Sungkyunkwan University, Suwon 16419, Republic of Korea*
[2]*School of Physics Science and Engineering, Tongji University, Shanghai 200092, China*
[3]*Theoretical Physics Department, CERN, 1211 Geneva 23, Switzerland*

We study the formation of primordial black holes and the generation of gravitational waves in a class of cosmological models that are direct supersymmetric analogs of the observationally favored nonminimally coupled Higgs inflation model. It is known that this type of model naturally includes multiple scalar fields which may be regarded as the inflaton. For the sake of simplicity we focus on the case where the inflaton field space is two dimensional. We analyze the multifield dynamics and find the region of parameters that gives copious production of primordial black holes that may comprise a significant part of the present dark matter abundance. We also compute the spectrum of the gravitational waves and discuss their detectability by means of future ground-based and space-borne gravitational wave observatories.

I. INTRODUCTION

In the radiation dominant era of the early Universe, the horizon mass in a Hubble volume may collapse to form a black hole if the density contrast is large enough. Such primordial black holes (PBHs) can exist in a much wider mass spectrum than the black holes resulting from the standard stellar evolution, and are a subject of active investigation since they were first postulated in the 1960s [1–4]. After the direct detection of gravitational waves by the LIGO and Virgo collaborations [5–7], PBHs received renewed interest as several groups suggested that the source of the detected gravitational waves could be binary black holes of primordial origin; see, e.g., [8–13] for a review. PBHs interact only through gravitation and are an excellent candidate of dark matter. The abundance of PBHs is constrained by observation, e.g., microlensing, as well as by theoretical consistency, e.g., successful big bang nucleosynthesis. While it is now well known that the PBHs of LIGO-Virgo event mass scale $\sim 30 M_\odot$ cannot account for the total dark matter abundance of the present Universe (see, e.g., [14]), there remains a mass window [11,15] at the asteroid scale 3.5×10^{-17}–$4 \times 10^{-12} M_\odot$ in which the whole

or a significant part of today's dark matter abundance may be attributed to PBHs.

Production of PBHs requires a large density contrast, much larger than that at the horizon exit scale of the cosmic microwave background (CMB). An important recent theoretical development is that if such large density contrast is present, gravitational waves are generated at the second order in perturbation theory [16–19], which may be large enough to be detected by future gravitational wave observatories; see, e.g., [10,20–24] for a review. If such gravitational waves are to be detected in the future, that would certainly mark a new era of cosmology, but even the null result would also give important constraints on the physics of the early Universe.

The power spectrum of the density perturbation needed for the production of PBHs is estimated to be seven orders of magnitude larger than that at the CMB scale, and thus it is a major theoretical challenge to build a model that naturally realizes the necessary enhancement of the power spectrum at small scales. Single field inflation with an inflection point is known to have the desired feature, and thus far many models for enhancement of the scalar power spectrum have been proposed; in some models, the enhancement is strong enough and abundant PBHs are produced, so that the PBHs may be considered as the dark matter of the Universe. One example is the single field model involving nonminimal Gauss-Bonnet coupling [25], in which the inflection-point like structure is maintained by the balance between the potential term and the Gauss-Bonnet coupling term [26].

High energy theories like string theory and supergravity naturally involve multiple scalar fields, and thus it seems fruitful to investigate possible production mechanisms of

*kawai@skku.edu
†Corresponding Author.
jinsu.kim@cern.ch

PBHs using the rich structure of the multifield dynamics. Such studies, in turn, will be able to constrain the UV physics if PBHs are to be found in the future within predicted mass ranges. There are many studies on PBHs and/or the associated gravitational waves in multifield inflation models, including [27–54]. Of these, the hybrid inflation type models are of particular interest, since many phenomenological models of particle physics indeed have such structure. A well-known drawback of the hybrid inflation model is that its original version predicts an observationally disfavored blue scalar spectrum $n_s \gtrsim 1$, and viable scenarios of hybrid inflation typically involve some correction terms, rendering the scenarios less predictive.

Below, we discuss production of PBHs and generation of gravitational waves in a supergravity-based scenario of cosmic inflation that seems to have eluded attention, but still has interesting features. The model involves multiple fields, but in one limit it approaches a single field model in which the effective potential becomes identical to that of the nonminimally coupled Higgs inflation model [55,56], which predicts observationally favored scalar spectral index $n_s \sim 0.97$ and small tensor-to-scalar ratio $r \ll 1$. Adjusting the parameters originating from the Kähler potential, the model resembles the hybrid inflation model; nevertheless the CMB spectrum still remains observationally favored. Like in other known scenarios of inflationary cosmology that generate PBHs, some degree of fine tuning is necessary in our model, and we show that sufficient enhancement of the scalar power is achieved by tuning some noncanonical (higher order) terms in the Kähler potential. We show this by carrying out detailed numerical study on two sets of benchmark parameter values.

We start in the next section with the description of the inflationary model. In Sec. III we show the dynamics of inflation, and in Sec. IV we comment on the behavior of the curvature power spectrum. Section V shows our analysis of the PBH production and the gravitational wave spectrum. We conclude in Sec. VI with brief comments.

II. NONMINIMALLY COUPLED SUPERGRAVITY INFLATION

Let us start with the supergravity Lagrangian

$$\mathcal{L} \supset \int d^4\theta \phi^\dagger \phi K + \left\{ \int d^2\theta \phi^3 W + \text{H.c.} \right\}, \quad (1)$$

where ϕ is the conformal compensator, W is the superpotential, and K is the Kähler potential in the superconformal framework. For our model it is essential that the superpotential includes a term

$$W \supset y S \bar{X} X, \quad (2)$$

where $(X, \bar{X})$ are a vectorlike pair of superfields and S is a singlet or an adjoint superfield under some gauge symmetry. While this structure is absent in the Minimal Supersymmetric Standard Model (MSSM), it is commonly found in supergravity embedding of particle theories beyond the Standard Model [57–72]. We allow the Kähler potential in the superconformal framework[1] to be slightly noncanonical, $K = -3M_\text{P}^2 \Phi$ with 71

$$\Phi = 1 - \frac{1}{3M_\text{P}^2}(|S|^2 + |\bar{X}|^2 + |X|^2) + \frac{\gamma}{2M_\text{P}^2}(\bar{X}X + \text{H.c.})$$
$$+ \frac{\sqrt{2}\kappa_3}{3M_\text{P}^3}(S^2 S^* + \text{H.c.}) + \frac{\kappa_4}{3M_\text{P}^4}|S|^4 + \frac{\kappa_6}{3M_\text{P}^6}|S|^6. \quad (3)$$

The third term proportional to γ gives rise to the non-minimal coupling, and the real constants κ_3, κ_4, and κ_6 represent the parameter freedom of the model that are adjustable as long as they are not ridiculously large.

Let us parametrize the flat direction h and the singlet direction s along the scalar components of the multiplets

$$X = \frac{h}{2}, \qquad \bar{X} = \frac{h}{2}, \qquad S = \frac{s}{\sqrt{2}}. \quad (4)$$

In many examples of concrete inflationary models, the inflaton trajectories are known to be stable along the real directions of s and h, and we thus restrict s and h to take real values below. Then the superpotential and the Kähler potential read, setting $M_\text{P} = 1$ henceforth,

$$W = \frac{y}{4\sqrt{2}} s h^2, \quad (5)$$

$$\Phi = 1 - \frac{1}{6}s^2 + \xi h^2 + \frac{\kappa_3}{3}s^3 + \frac{\kappa_4}{12}s^4 + \frac{\kappa_6}{24}s^6, \quad (6)$$

where

$$\xi = \frac{\gamma}{4} - \frac{1}{6}. \quad (7)$$

Of course, other terms, such as the ones in the MSSM, may be present in the theory but these will be neglected below, with assumption that the initial vacuum expectation values of the scalar components of the multiplets other than s and h are sufficiently small.

The Lagrangian in the Einstein frame is obtained by the Weyl transformation of the metric. It reads

$$\mathcal{L}_\text{E} = \sqrt{-g}\left[\frac{1}{2}R - \frac{1}{2}G_{ab}g^{\mu\nu}\partial_\mu\varphi^a\partial_\nu\varphi^b - V_\text{E}\right], \quad (8)$$

---

[1]The Kähler potential in the Einstein frame is $\mathcal{K} = -3M_\text{P}^2 \ln \Phi$. We choose the mass scale of the supergravity to be the reduced Planck scale $M_\text{P} = 2.44 \times 10^{18}$ GeV.

where $\varphi^a = (h, s)$ and the components of the field space metric are

$$G_{hh} = \frac{6\xi^2 h^2 + \Phi}{\Phi^2}, \tag{9}$$

$$G_{hs} = -\frac{\xi h s}{\Phi^2}\left(1 - 3\kappa_3 s - \kappa_4 s^2 - \frac{3}{4}\kappa_6 s^4\right), \tag{10}$$

$$G_{ss} = \frac{1}{\Phi^2}\left[\frac{4s^4(2\kappa_3^2 + \kappa_4) + \kappa_6 s^6(8 - 8\kappa_3 s - \kappa_4 s^2)}{48}\right.$$
$$\left. + (1 + \xi h^2)\left(1 - 4\kappa_3 s - 2\kappa_4 s^2 - \frac{9}{4}\kappa_6 s^4\right)\right]. \tag{11}$$

The two dimensional field space (s, h) is curved. The scalar potential in the Einstein frame is

$$V_{\rm E} = \frac{V_{\rm J}}{\Phi^2}, \tag{12}$$

where

$$V_{\rm J} = \frac{y^2 h^2 s^2}{4} + \frac{y^2 h^4}{4d(s)} + \frac{y^2 h^4 s^2 [\frac{3}{2}\gamma - f(s)]^2}{24 - 6\gamma h^2 + 9\gamma^2 h^2 + g(s)}, \tag{13}$$

with

$$d(s) = 4(1 - 4\kappa_3 s - 2\kappa_4 s^2) - 9\kappa_6 s^4, \tag{14}$$

$$g(s) = \frac{8(2\kappa_3^2 + \kappa_4)s^4 + 16\kappa_6 s^6 - 16\kappa_3\kappa_6 s^7 - 2\kappa_4\kappa_6 s^8}{d(s)}, \tag{15}$$

$$f(s) = \frac{2(\kappa_3 + \kappa_4 s)s + 3\kappa_6 s^4}{d(s)}. \tag{16}$$

Formalisms for multifield inflation have been developed by many authors, including [73–80]. Here we simply list a few key equations; see, e.g., Appendix A of [61] for more explanation. The background evolution is described by the equations of motion for the multifields,

$$\frac{D\dot{\varphi}^a}{dt} + 3H\dot{\varphi}^a + G^{ab}\nabla_b V(\varphi^c) = 0, \tag{17}$$

together with the Friedmann equation

$$3H^2 = \frac{1}{2}G_{ab}\dot{\varphi}^a\dot{\varphi}^b + V(\varphi^c). \tag{18}$$

The overdot is the derivative with respect to the cosmic time, D stands for covariantized time derivative, and ∇ stands for the covariantized field space derivative.

On a given background, the dynamics of the perturbations is found by solving the equations

$$\ddot{Q}_\sigma + 3H\dot{Q}_\sigma + \left[\frac{k^2}{a^2} + \mathcal{M}_{\sigma\sigma} - \omega^2 - \frac{1}{a^3}\frac{d}{dt}\left(\frac{a^3\dot{\sigma}^2}{H}\right)\right]Q_\sigma$$
$$= 2\frac{d}{dt}(\omega Q_s) - 2\left(\frac{V_{,\sigma}}{\dot{\sigma}} + \frac{\dot{H}}{H}\right)\omega Q_s, \tag{19}$$

$$\ddot{Q}_s + 3H\dot{Q}_s + \left[\frac{k^2}{a^2} + \mathcal{M}_{ss} + 3\omega^2\right]Q_s$$
$$= 4\frac{\omega}{\dot{\sigma}}\frac{\dot{H}}{H}\left[\frac{d}{dt}\left(\frac{H}{\dot{\sigma}}Q_\sigma\right) - \frac{2H}{\dot{\sigma}}\omega Q_s\right], \tag{20}$$

where Q_σ and Q_s are respectively the adiabatic and entropic perturbations, and

$$\dot{\sigma} \equiv \sqrt{G_{ab}\dot{\varphi}^a\dot{\varphi}^b}, \tag{21}$$

$$\hat{\sigma}^a \equiv \frac{\dot{\varphi}^a}{\dot{\sigma}}, \tag{22}$$

$$\omega^a \equiv \frac{d\hat{\sigma}^a}{dt} + \Gamma^a_{bc}\dot{\varphi}^b\hat{\sigma}^c, \tag{23}$$

$$\hat{s}^a \equiv \frac{\omega^a}{|\omega^a|}, \tag{24}$$

$$\mathcal{M}_{\sigma\sigma} \equiv \hat{\sigma}_a\hat{\sigma}^b\mathcal{M}^a_b, \tag{25}$$

$$\mathcal{M}_{ss} \equiv \hat{s}_a\hat{s}^b\mathcal{M}^a_b, \tag{26}$$

$$\mathcal{M}^a_b \equiv G^{ac}\nabla_b\nabla_c V - \mathcal{R}^a_{\ cdb}\dot{\varphi}^c\dot{\varphi}^d, \tag{27}$$

$$V_{,\sigma} \equiv \hat{\sigma}^a\nabla_a V. \tag{28}$$

Here $\mathcal{R}^a_{\ cdb}$ is the field space Riemann tensor. The curvature and isocurvature perturbations are then defined as follows:

$$\mathcal{R} = \frac{H}{\dot{\sigma}}Q_\sigma, \qquad \mathcal{S} = \frac{H}{\dot{\sigma}}Q_s. \tag{29}$$

III. INFLATON TRAJECTORIES

We focus on the "cubic Kähler potential model" where κ_6 is set to be zero and the "sextic Kähler potential model" where $\kappa_3 = 0$. Furthermore we assume that the inflationary trajectory starts in the large-h limit with a small s-field value. In other words we study effects of the s field on the otherwise standard single field nonminimal inflation model.[2]

For both cubic and sextic cases we initially have eight free parameters; four potential parameters (κ_3 or $\kappa_6, \kappa_4, \xi, y$), two initial field values ($h_{\rm ini}, s_{\rm ini}$), and two initial velocities

---

[2]Taking $s = 0$, we recover the standard nonminimally coupled Higgs inflation which is known to give observationally favored prediction of the CMB spectrum.
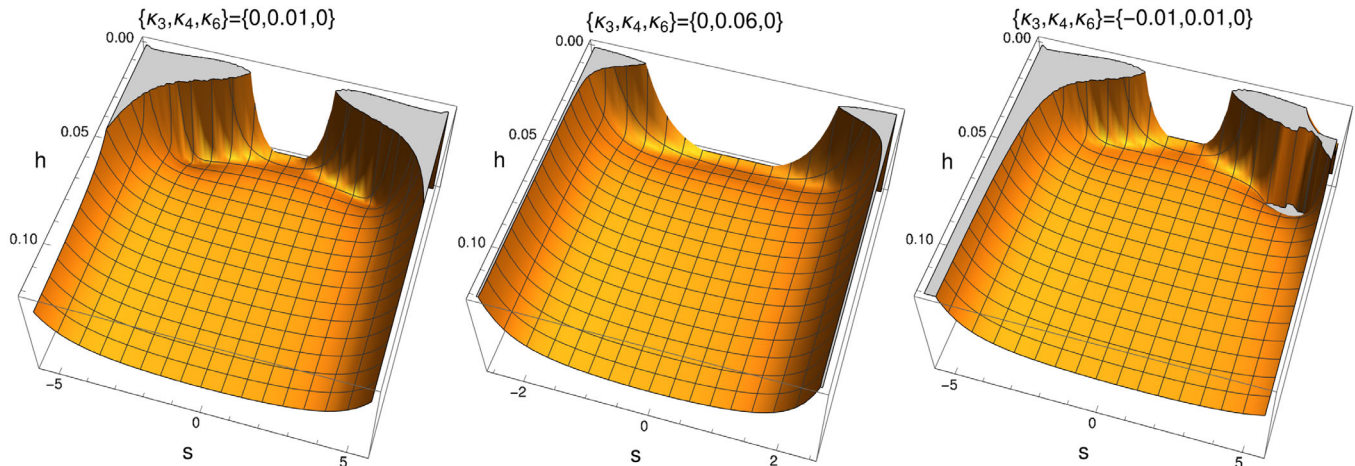
FIG. 1. Typical shapes of the Einstein frame potential $V_{\rm E}$ for the cubic case ($\kappa_6 = 0$). From left to right we have set $\{\kappa_3, \kappa_4\} = \{0, 0.01\}$, $\{0, 0.06\}$, and $\{-0.01, 0.01\}$, with $\xi = 10^4$. For smaller values of κ_4 the potential develops two extra minima at $s \neq 0$. The κ_3 parameter introduces an asymmetry and tilts the scalar potential in the s-field direction.

($\dot{h}_{\rm ini}$, $\dot{s}_{\rm ini}$). For the initial velocities, we use the slow roll background equations of motion which is a good approximation in the large-h limit. The parameter y enters in the potential as an overall factor. We thus use y to match the magnitude of the curvature power spectrum at the pivot scale, namely $\mathcal{P}_\zeta(k_*) \approx 2 \times 10^{-9}$. The current observational bound on the isocurvature perturbations is safely satisfied in our model. Finally, the initial s-field value is chosen to be at the potential minimum at $h = h_{\rm ini}$, and $h_{\rm ini}$ is set to be 0.12 which is enough to achieve $60 e$-folds. We are thus left with three parameters (κ_3 or κ_6, κ_4, ξ). For simplicity, we assume that after inflation the Universe undergoes immediate transition to radiation domination.[3]

A. Cubic case

To ensure the stability of the scalar potential the quartic term needs to be positive, i.e., $\kappa_4 > 0$. Typical shapes of the Einstein frame potential (12) are shown in Fig. 1. One may see that, as the κ_4 parameter becomes smaller, two additional minima at $s \neq 0$ start to appear in the potential, as was pointed out in [58]. Turning on κ_3 makes the scalar potential tilted to one side in the s-field direction, introducing an asymmetry. Choosing an appropriate value for κ_3, we may adjust the inflaton trajectory in such a way that

it passes the saddle point between the true vacuum at $s = 0$ and the false vacuum[4] at $s \neq 0$.

We show three examples of the inflaton trajectory for different values of κ_3 in Fig. 2, fixing $\kappa_4 = 0.01$ and $\xi = 10^4$. When $\kappa_3 = 0$, we obtain a straight trajectory, while for a negatively large value of κ_3, the trajectory falls into a false vacuum at $s \neq 0$.[5] With an appropriate κ_3 value, the inflaton trajectory crosses the saddle point between the false vacuum and the true vacuum at $s = 0$ as shown in the middle in Fig. 2. When the trajectory crosses the saddle point, the first Hubble slow roll parameter $\epsilon_1 \equiv -\dot{H}/H^2$ gets suppressed as shown in Fig. 3, indicating the ultraslow roll regime. It hints at the possibility of curvature perturbation enhancement and thus PBH formations.

From the perturbation equation for the entropic perturbation (20), the effective entropic mass squared is defined as $\mu_s^2 \equiv \mathcal{M}_{ss} + 3\omega^2$. As the inflaton trajectory crosses the saddle point μ_s^2 becomes negative as shown in Fig. 4. In other words the entropic perturbation briefly enters the tachyonic regime, sourcing the growth of the perturbation. The growth of the entropic perturbation in turn may source the curvature perturbation. This is a unique feature of multifield inflation.

B. Sextic case

In the sextic case, $\kappa_6 > 0$ is required for the stability of the scalar potential. Figure 5 shows typical Einstein frame potential shapes. Note that, unlike the cubic case, $s = 0$ is not a stable point at $h = h_{\rm ini}$. Similar to the cubic case, when

---

[3]The effects of the delay of thermalization due to noninstantaneous reheating would only change the number of e-folds from our choice of 60. Deviation of the e-folding number would slightly change the value of the y parameter and hence the spectral index n_s and the tensor-to-scalar ratio r. However, for the class of inflationary models we consider, the change is known to be small and safely within current observational bounds of the latest Planck [81] and BICEP/Keck [82] observations. In single-field models, this is discussed for example in Ref. [72].

[4]Although somewhat misnamed, we refer to the minimum at $s = 0$ as the "true vacuum" and the minimum at $s \neq 0$ as the "false vacuum," regardless of the potential values at these points.

[5]For positively large values of κ_3, the potential becomes tilted in the opposite direction, and thus the trajectory falls into a false vacuum at $s < 0$. We do not consider this case.
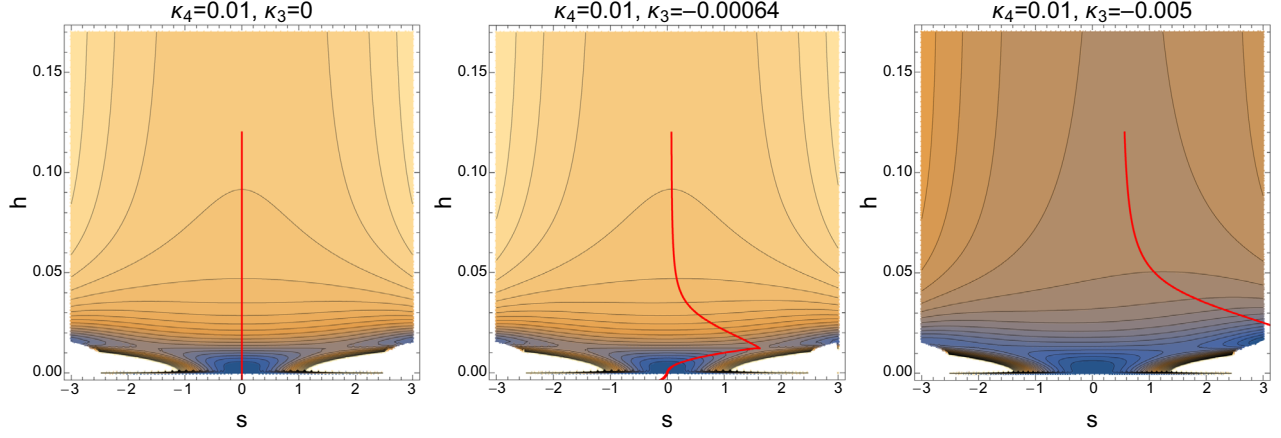
FIG. 2. Examples of the inflaton trajectory for the cubic case $(\kappa_6 = 0)$. From left to right $\kappa_3 = 0$, -0.00064, and -0.005, with $\kappa_4 = 0.01$ and $\xi = 10^4$. The initial condition for the h field is set to be 0.12. The initial s-field value is chosen to be at the potential minimum at $h = 0.12$. The initial field velocities are fixed by using the slow roll background equations of motion. As κ_3 introduces a tilt in the scalar potential along the s-field direction, the inflaton trajectory deviates from a straight line. For a large negative κ_3 value, the trajectory falls into a false vacuum. With an appropriate value of κ_3, the inflaton trajectory may cross the saddle point between the false vacuum at $s \neq 0$ and the true vacuum at $s = 0$ as shown in the middle.
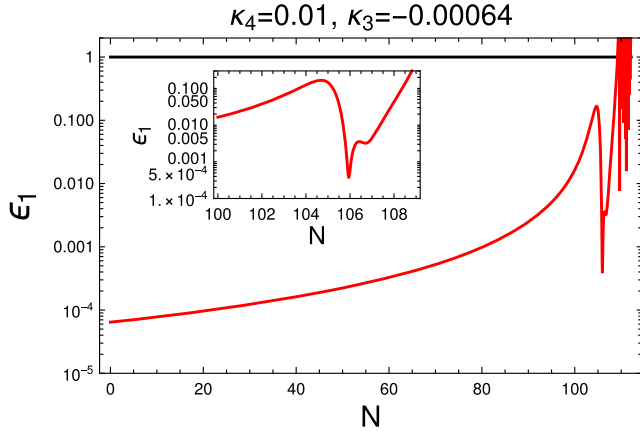
FIG. 3. First Hubble slow roll parameter for $\kappa_3 = -0.00064$ and $\kappa_4 = 0.01$. As the inflaton trajectory crosses the saddle point ϵ_1 gets suppressed, entering the ultraslow roll regime.
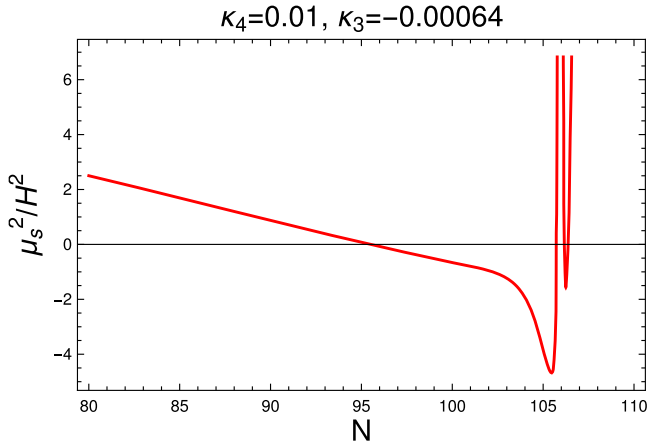
FIG. 4. Effective entropic mass squared for $\kappa_3 = -0.00064$ and $\kappa_4 = 0.01$. As the inflaton trajectory crosses the saddle point the entropic mass squared becomes negative, i.e., tachyonic.

$\kappa_4 = 0$, smaller values of κ_6 introduce false vacua at $s \neq 0$. The role of the κ_4 parameter is twofold. One is to shift the potential minimum in the large-h limit toward a larger s-field value. The other is to create or deepen false vacua at $s \neq 0$.

We present four samples of the inflaton trajectory for different values of κ_4 in Fig. 6 with $\kappa_6 = 0.5$ and $\xi = 10^4$. One can clearly see the effect of κ_4; once κ_4 takes a negatively large value, the inflaton trajectory gets trapped in the false vacuum. Adjusting the value of κ_4, we may balance the heights of the false vacuum and the true vacuum. In this case the inflaton undergoes an ultraslow roll regime. This case demonstrated in Fig. 7 which shows the first Hubble slow roll parameter ϵ_1. Similar to the cubic case we observe the suppression of ϵ_1 near the ultraslow roll regime which may lead to the enhancement of the curvature perturbation. Moreover the tachyonic behavior is also seen in the sextic case although the degree is less significant compared to the cubic case. Thus the sextic case as well has the possibility of PBH formations.

IV. CURVATURE POWER SPECTRUM

The suppression of the slow roll parameter ϵ_1 suggests the possibility of curvature perturbation enhancement. In this section we demonstrate that this is indeed the case. To compute the curvature power spectrum $\mathcal{P}_\zeta(k)$ we adopt the transport method[6] [83,84,89–95], which, with the assumption of instantaneous reheating and small isocurvature mode, evolves the system from deep inside the horizon[7] until the end of inflation specified by the condition $\epsilon_1 = 1$.

---

[6]Packages implementing the transport method are publicly available, including mTransport [83], CppTransport [84,85], PyTransport [84,86,87], and Inflation.jl [88].

[7]We have chosen 8e-foldings before the horizon exit and checked convergence for larger values.
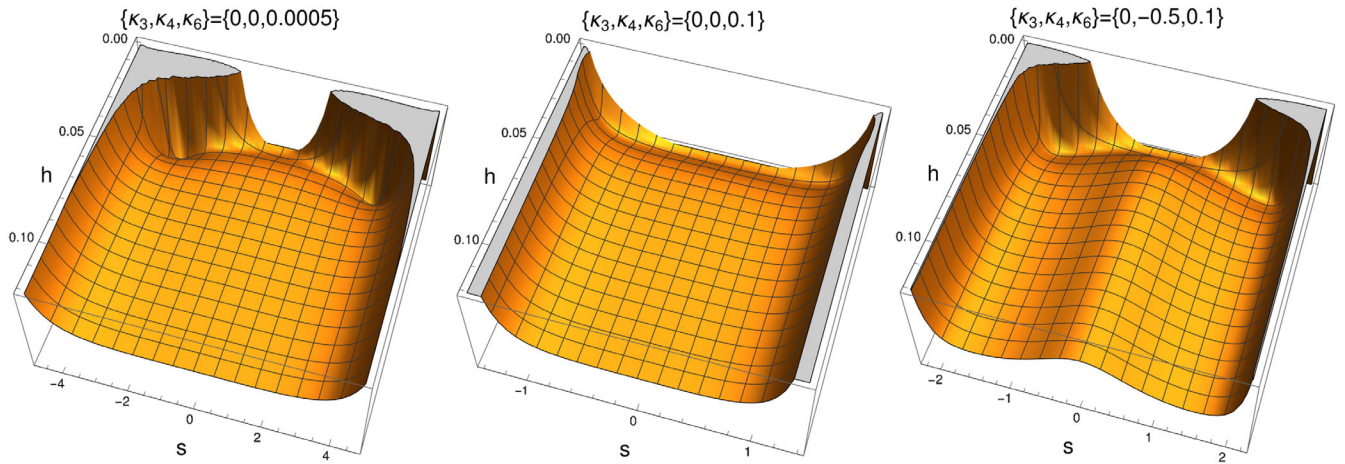
FIG. 5. First Hubble slow roll parameter for $\kappa_6 = 0.5$ and $\kappa_4 = -0.96$. The suppression of ϵ_1 indicates the curvature power spectrum enhancement and thus PBH formations.
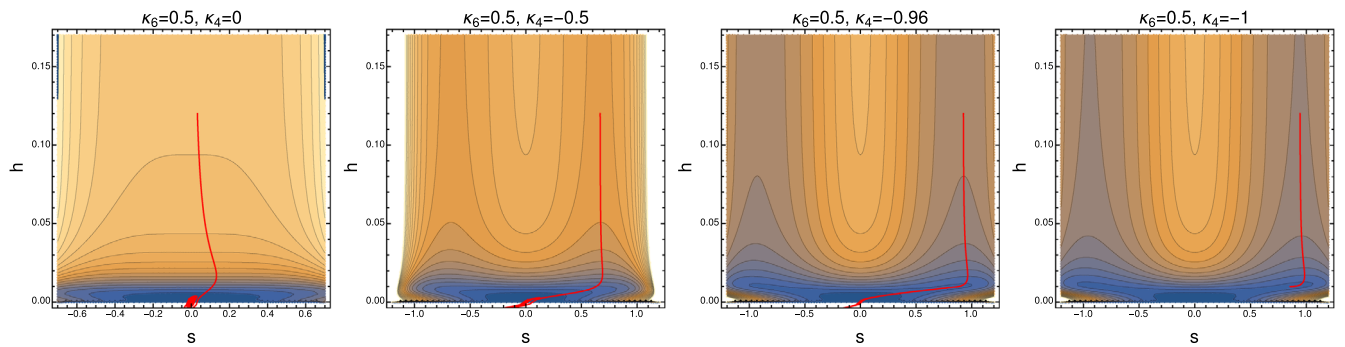
FIG. 6. Examples of the inflaton trajectory for the sextic case ($\kappa_3 = 0$). From left to right $\kappa_4 = 0, -0.5, -0.96$, and -1, with $\kappa_6 = 0.5$ and $\xi = 10^4$. The initial condition for the h field is set to be 0.12. The initial s-field value is chosen to be at the potential minimum at $h = 0.12$. The initial field velocities are fixed by using the slow roll background equations of motion. Note that, unlike the cubic case, $s = 0$ is no longer a stable position at h_{ini}. As κ_4 negatively increases, the false vacuum at $s \neq 0$ becomes deeper than the true vacuum at $s = 0$; for example, we see that the inflaton trajectory gets trapped at the false vacuum when $\kappa_4 = -1$. With an appropriate κ_4 value, one may balance between the false vacuum and the true vacuum, generating an ultraslow roll regime.
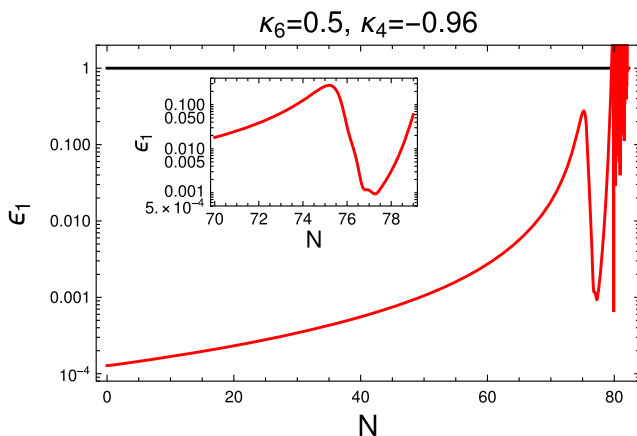
FIG. 7. Typical shapes of the Einstein frame potential V_E for the sextic case ($\kappa_3 = 0$). From left to right we have set $\{\kappa_4, \kappa_6\} = \{0, 0.0005\}$, $\{0, 0.1\}$, and $\{-0.5, 0.1\}$, with $\xi = 10^4$.

In Fig. 8 the curvature power spectrum, normalized by its value at the pivot scale, is shown as a function of the wave number for different values of κ_3 and κ_4 for the cubic case. For all the cases we have set $\xi = 10^4$. We can see that, for a fixed value of κ_4, the κ_3 parameter controls the magnitude as well as the peak position of the enhancement. For a fixed value of the curvature power spectrum, say $\mathcal{P}_\zeta(k)/\mathcal{P}_\zeta(k_*) = 10^6$, the κ_4 parameter controls the position of the peak; the peak position moves toward a smaller wave number as κ_4 increases.

Figure 9 shows the curvature power spectrum, normalized by its value at the pivot scale as a function of the wave number for different values of κ_4 and κ_6 for the sextic case. We have again set $\xi = 10^4$. Similar to the cubic case, the peak position and the magnitude of the enhancement are controlled by the κ_4 parameter for a fixed value of κ_6. On the other words, the κ_6 parameter is the key controller of the peak position for a fixed value of the curvature power spectrum; in this case, unlike the cubic
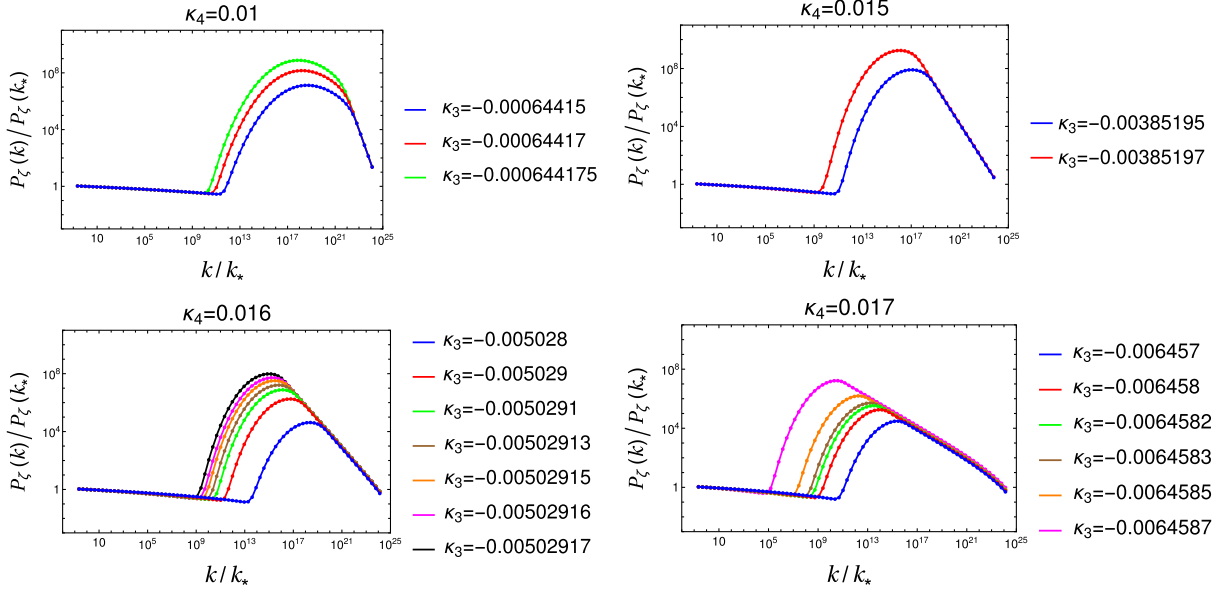
FIG. 8. Curvature power spectrum for the cubic case. For a fixed value of κ_4, the peak position and the magnitude of the enhancement are controlled by the κ_3 parameter. For a fixed value of the curvature power spectrum, the peak position is controlled by the κ_4 parameter. As κ_4 increases, the peak position moves toward a lower wave number.
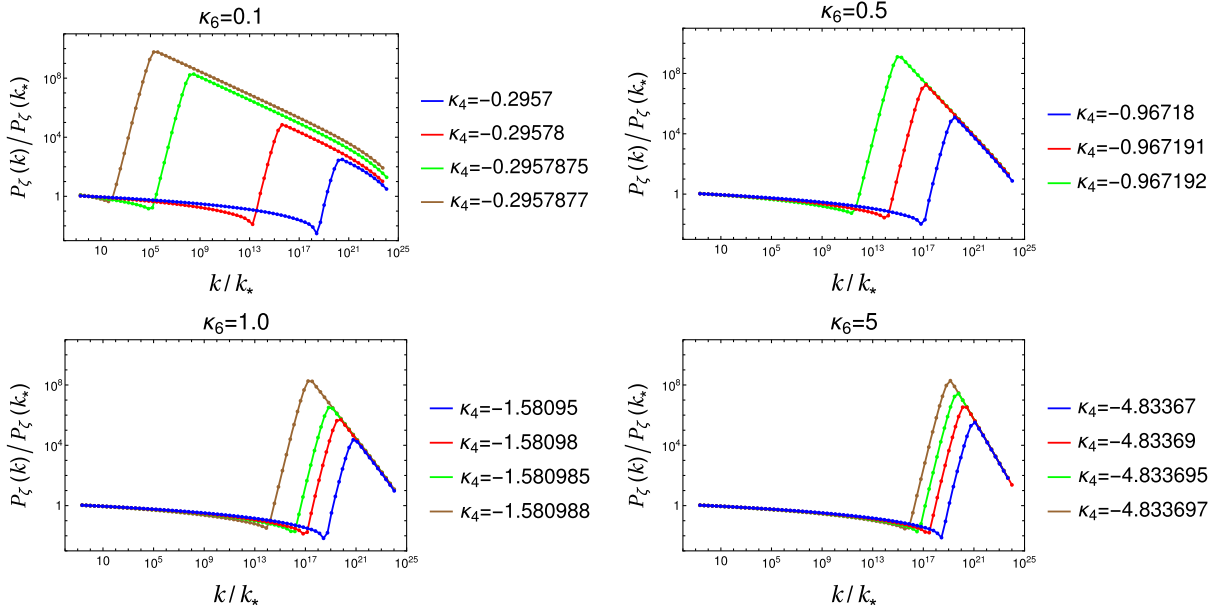
FIG. 9. Curvature power spectrum for the sextic case. For a fixed value of κ_6, the peak position and the magnitude of the enhancement are controlled by the κ_4 parameter. For a fixed value of the curvature power spectrum, the peak position is controlled by the κ_6 parameter. As κ_6 increases, the peak position moves toward a higher wave number.

case, the peak position moves toward a larger wave number as κ_6 increases.

V. PREDICTION OF THE MODEL AND FUTURE DETECTABILITY

As a consequence of the curvature perturbation enhancement, PBHs may form through the gravitational collapse at

the horizon reentry and constitute a large part of the today's dark matter relic density. Another consequence is the generation of scalar-sourced stochastic gravitational waves at the nonlinear order. In this section we discuss the prediction of the model on the formation of PBHs and the generation of the gravitational waves. Aligning with the assumption of instantaneous reheating, we consider that the
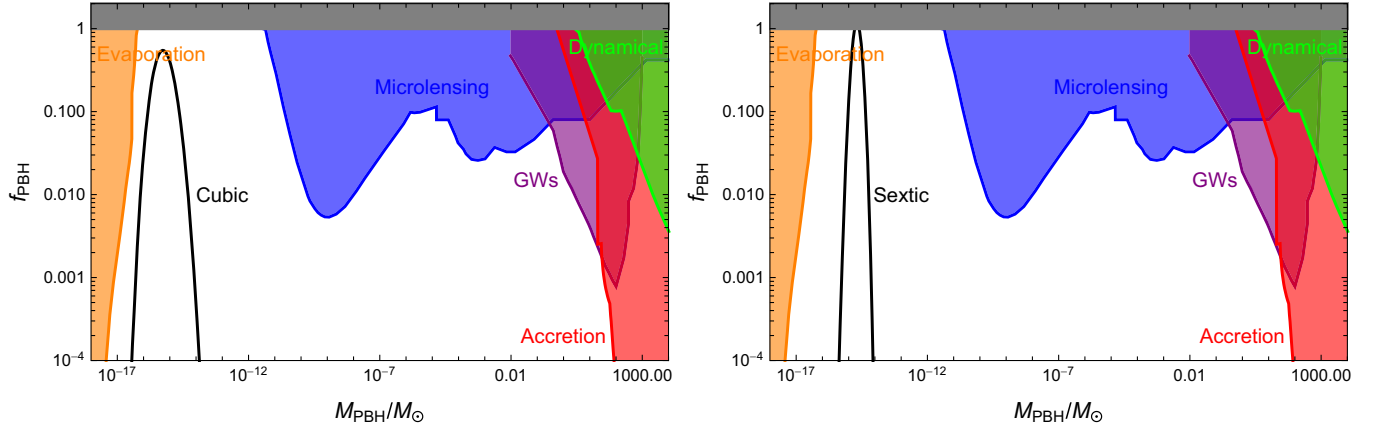
FIG. 10. The spectrum of the produced PBHs. The left panel shows the case for the cubic model, where $\kappa_4 = 0.0163$ is chosen, and κ_3 is tuned to match $f_{PBH}^{tot} \approx 1$. The right panel is the sextic model, where $\kappa_6 = 0.2$ is chosen, and κ_4 is tuned to match $f_{PBH}^{tot} \approx 1$. We consulted [12,121] for the constraints data. See also Refs. [122–124] for additional constraints such as those coming from gamma-ray observations and the global 21 cm signal, and Ref. [125] for forecasted constraints from future gamma-ray telescopes.

PBH formation and the generation of the gravitational waves happen during the radiation-dominated era.[8]

A. Primordial black holes

The produced PBHs have the mass of

$$M = \gamma M_{H,0} \Omega_{rad,0}^{1/2} \left(\frac{g_{*,0}}{g_{*,f}}\right)^{1/6} \left(\frac{k_0}{k_f}\right)^2, \qquad (30)$$

at the formation time, where $M_{H,0} = 4\pi/H$ is the horizon mass, Ω_{rad} is the radiation energy density parameter, g_* is the effective degrees of freedom, the subscript f (0) denotes the formation time (today), and the factor γ describes the fraction of the horizon mass that turns into the PBHs. Following simple analytical estimations [96] we use $\gamma = 0.2$.

The energy density of the PBHs today can be obtained by redshifting that at the formation time, namely $\rho_{PBH,0} = \rho_{PBH,f}(a_f/a_0)^3 \approx \gamma\beta\rho_{rad,f}(a_f/a_0)^3$, since the PBHs behave as matter. Here β denotes the probability of the density fluctuation $\delta > \delta_c$, which is given by

$$\beta = \int_{\delta_c} d\delta \frac{1}{\sqrt{2\pi\sigma^2}} \exp\left(-\frac{\delta^2}{2\sigma^2}\right), \qquad (31)$$

where $\delta_c = 1/3$ [96] is a threshold value and σ^2 is the variance [97,98]

$$\sigma^2 = \frac{16}{81} \int_0^\infty \frac{dq}{q} \left(\frac{q}{k}\right)^4 W^2\left(\frac{q}{k}\right) \mathcal{P}_\zeta(q). \qquad (32)$$

Note that we have assumed a Gaussian density fluctuation, neglecting possible effects of non-Gaussianities [99–120], and we take the Gaussian function for the window function $W(q/k) = \exp(-(q/k)^2/2)$.

The total abundance is $\Omega_{PBH,tot} = \int d\ln M \Omega_{PBH}$, with Ω_{PBH} expressed in terms of f_{PBH} which is given by

$$f_{PBH} \equiv \frac{\Omega_{PBH,0}}{\Omega_{CDM,0}}$$

$$\approx \left(\frac{\beta}{3.27 \times 10^{-8}}\right)\left(\frac{\gamma}{0.2}\right)^{\frac{3}{2}}\left(\frac{106.75}{g_{*,f}}\right)^{\frac{1}{4}}$$

$$\times \left(\frac{0.12}{\Omega_{CDM,0}h^2}\right)\left(\frac{M}{M_\odot}\right)^{-\frac{1}{2}}, \qquad (33)$$

where $\Omega_{CDM,0}$ is the today's density parameter of the cold dark matter, h is the rescaled Hubble rate today, and $M_\odot$ is the solar mass.

In Fig. 10 we present two benchmark points for the PBH spectrum for the cubic and sextic cases. For the cubic case $\kappa_4 = 0.0163$ is chosen and κ_3 is tuned to match f_{PBH}^{tot} to be unity. For the sextic model we chose $\kappa_6 = 0.2$, and κ_4 is tuned so that f_{PBH}^{tot} becomes unity. Thus both the cubic and sextic models may produce enough PBHs to constitute all of the current dark matter abundance.

Figure 11 shows the dependence on the parameters κ_4 and κ_3 for the cubic model case (the left panel) and on the parameters κ_6 and κ_4 for the sextic model case (the right panel). With these parameters the peak frequency of the enhanced perturbations shifts, and thus the resulting PBH mass spectrum also changes. The observationally viable parameters are then constrained by the evaporation bounds

---

[8]The effects of noninstantaneous reheating, which are model-dependent, can be absorbed by a slight shift in the number of e-folds and do not alter the conclusion of our paper; see also footnote 3. Note further that the relative scale between the CMB and the mode corresponding to PBHs and gravitation waves are insensitive to the reheating process.
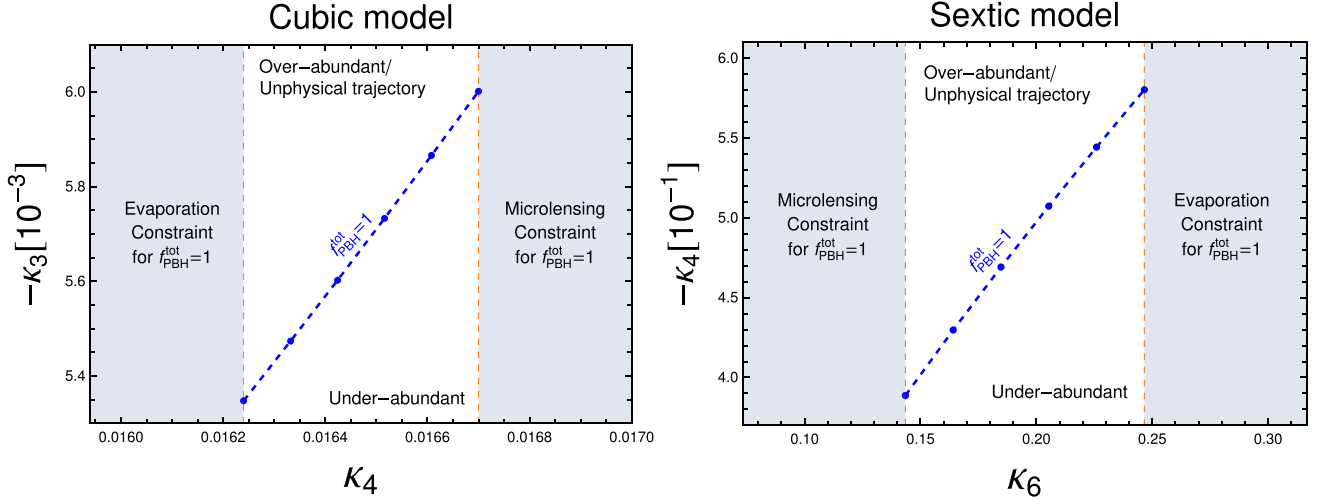
FIG. 11. The dashed line indicates the parameters (κ_4, κ_3) of the cubic mode (the left panel) and the (κ_6, κ_4) of the sextic model giving $f_{\text{PBH}}^{\text{tot}} = 1$, namely the primordial black holes comprise the total dark matter abundance today. The region below the line corresponds to underabundance. The region above the line corresponds to overabundant PBHs and the trajectories that fall into one of the non-Standard Model vacua (we call them false vacua) as shown in the rightmost panels of Figs. 2 and 6, but the overabundance region is so narrow that it is not recognizable.

and the microlensing bounds, see Fig. 10. We have found $0.01624 \lesssim \kappa_4 \lesssim 0.01670$ for the cubic model and $0.1435 \lesssim \kappa_6 \lesssim 0.2466$ for the sextic model. In both panels, the dashed line indicates the model parameters yielding the PBHs corresponding to the total dark matter abundance ($f_{\text{PBH}}^{\text{tot}} = 1$). The region under the line corresponds to $f_{\text{PBH}}^{\text{tot}} < 1$. The region above the line corresponds to trajectories that fall into one of the minima that does not represent our Universe. There is a region right above the line that gives overabundant PBH $f_{\text{PBH}}^{\text{tot}} > 1$, which is too narrow to be visible.

As one can see from Fig. 11, the production rate $f_{\text{PBH}}^{\text{tot}}$ is rather sensitive to the choice of the Kähler potential parameters κ_3, κ_4, κ_6. This type of sensitivity is a common feature in similar inflationary production mechanisms of primordial black holes. Since our scenario is based on supersymmetry, the prediction, while sensitive to the parameters, is robust against radiative corrections compared to other scenarios without supersymmetry.

B. Induced gravitational waves

In the subhorizon region the gravitational waves have the energy density of [126,127]

$$\rho_{\text{GW}} = \frac{1}{16a^2} \langle \overline{\partial_k h_{ij} \partial^k h^{ij}} \rangle, \tag{34}$$

where the overline denotes the average over oscillations. Let us decompose the tensor h_{ij} as

$$h_{ij}(t, \mathbf{x}) = \int \frac{d^3 k}{(2\pi)^{3/2}} (h_{\mathbf{k}}^+(t) e_{ij}^+(\mathbf{k}) + h_{\mathbf{k}}^\times(t) e_{ij}^\times(\mathbf{k})) e^{i\mathbf{k}\cdot\mathbf{x}}, \tag{35}$$

where

$$e_{ij}^+(\mathbf{k}) = \frac{1}{\sqrt{2}} (e_i(\mathbf{k}) e_j(\mathbf{k}) - \bar{e}_i(\mathbf{k}) \bar{e}_j(\mathbf{k})), \tag{36}$$

$$e_{ij}^\times(\mathbf{k}) = \frac{1}{\sqrt{2}} (e_i(\mathbf{k}) \bar{e}_j(\mathbf{k}) + \bar{e}_i(\mathbf{k}) e_j(\mathbf{k})), \tag{37}$$

are the polarization tensors with $e_i(\mathbf{k})$ and $\bar{e}_i(\mathbf{k})$ being two orthogonal unit vectors. Using the expression (35) in the energy density (34) gives

$$\rho_{\text{GW}}(t) = \int d\ln k \, \frac{1}{8} \left(\frac{k}{a}\right)^2 \overline{\mathcal{P}_h(t, k)}. \tag{38}$$

Here $\mathcal{P}_h(t, k) \equiv \mathcal{P}_h^{+,\times}(t, k)$, defined by

$$\langle h_{\mathbf{k}}^+(t) h_{\mathbf{q}}^+(t) \rangle = \delta^3(\mathbf{k} + \mathbf{q}) \frac{2\pi^2}{k^3} \mathcal{P}_h^+(t, k), \tag{39}$$

$$\langle h_{\mathbf{k}}^\times(t) h_{\mathbf{q}}^\times(t) \rangle = \delta^3(\mathbf{k} + \mathbf{q}) \frac{2\pi^2}{k^3} \mathcal{P}_h^\times(t, k). \tag{40}$$

We note that $\mathcal{P}_h^+(t, k) = \mathcal{P}_h^\times(t, k)$. Omitting the polarization index, we define the gravitational wave energy density parameter as follows:

$$\Omega_{\text{GW}}(t, k) \equiv \frac{\rho_{\text{GW}}(t, k)}{\rho_{\text{crit}}} = \frac{1}{24} \left(\frac{k}{aH}\right)^2 \overline{\mathcal{P}_h(t, k)}. \tag{41}$$

To obtain the tensor power spectrum one may solve the tensor perturbation equation [19,128,129]
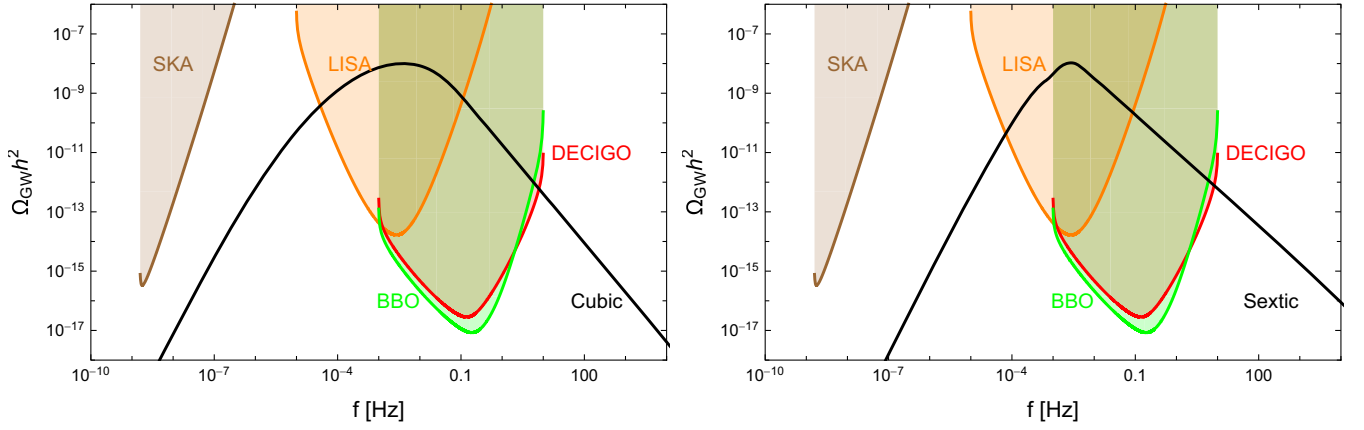
FIG. 12. The spectrum of the gravitational waves generated from the curvature perturbations. The left panel shows the cubic model and the right panel shows the sextic model. The chosen parameters are the same as those presented in Fig. 10. The data for the sensitivity curves are obtained from [144,145].

$$h''_{\mathbf{k}} + 2aHh'_{\mathbf{k}} + k^2h_{\mathbf{k}} = 4S_{\mathbf{k}}, \qquad (42)$$

where the prime denotes the derivative with respect to the conformal time. The source term $S_{\mathbf{k}}$ is given by

$$S_{\mathbf{k}} = \int \frac{d^3q}{(2\pi)^{3/2}} e_{ij}(\mathbf{k}) q_i q_j \left[2\Psi_{\mathbf{q}}\Psi_{\mathbf{k}-\mathbf{q}} \right.$$
$$\left. + \frac{4}{3(1+w)} (\mathcal{H}^{-1}\Psi'_{\mathbf{q}} + \Psi_{\mathbf{q}})(\mathcal{H}^{-1}\Psi'_{\mathbf{k}-\mathbf{q}} + \Psi_{\mathbf{k}-\mathbf{q}}) \right], \quad (43)$$

where w is the equation of state and $\Psi_{\mathbf{k}}$ is the Fourier transform of the scalar perturbation in the conformal Newtonian gauge where the metric is given by $ds^2 = -(1 + 2\Psi)dt^2 + a^2[(1 - 2\Psi)\delta_{ij} + h_{ij}/2]dx^i dx^j$ with the anisotropic stress tensor being neglected. We assume that the induced gravitational waves are generated in the radiation dominated era. Then, at the generation time, we obtain [128]

$$\Omega_{\mathrm{GW}}(t_{\mathrm{f}}, k) = \frac{1}{12} \int_0^\infty dv \int_{|1-v|}^{1+v} du \left(\frac{4v^2 - (1 + v^2 - u^2)^2}{4uv} \right)^2$$
$$\times \mathcal{P}_\zeta(kv)\mathcal{P}_\zeta(ku) \left(\frac{3(u^2 + v^2 - 3)}{4u^3v^3} \right)^2$$
$$\times \left[\left(-4uv + (u^2 + v^2 - 3)\log\left| \frac{3 - (u+v)^2}{3 - (u-v)^2} \right| \right)^2 \right.$$
$$\left. + \pi^2(u^2 + v^2 - 3)^2\theta(v + u - \sqrt{3}) \right]. \qquad (44)$$

Multiplying the present day radiation energy density parameter $\Omega_{\mathrm{rad},0}$, we find the energy density parameter today $\Omega_{\mathrm{GW}} = \Omega_{\mathrm{rad},0}\Omega_{\mathrm{GW}}(t_{\mathrm{f}})$ [128,130].

The spectrum of the scalar-sourced second order gravitational waves generated from the cubic and sextic models is shown in Fig. 12 together with the sensitivity curves for future experiments such as LISA [131,132], DECIGO [133–137], BBO [138–140], and SKA [141–143]. We observe that the signals are within the reach of LISA, DECIGO, and BBO.

VI. FINAL REMARKS

In this work we analyzed models of two-field inflation which are well motivated from high energy physics and particle phenomenology. We demonstrated by numerical studies that these models can produce primordial black holes during the radiation dominated era which are of interest as a candidate of the present day dark matter. We investigated two sample cases in detail, one with the Kähler potential including the cubic term of the singlet field, and the other with the sextic term of the singlet field. We have found that in both cubic and sextic cases significant enhancement of the curvature perturbation can be achieved. In both the cubic and sextic cases the enhancement can be large enough so that the produced primordial black holes are abundant enough to account for the whole present day dark matter abundance. We have also computed the spectrum of the gravitational waves resulting as the secondary effect of the large scalar perturbation. We have found that, for both cubic and the sextic cases, the model can generate gravitational waves in the target range of detectors, including LISA, DECIGO, and BBO.

The focus of this paper has been on the features of the Kähler potential and the trajectory of the inflaton that may lead to the production of primordial black holes. While we used the simple superpotential (2), this may be generalized to more realistic phenomenological examples. It would be certainly interesting to analyze various cases based on

specific particle physics models. For example, in the $SU(5)$ GUT model [61] the inflaton trajectory needs to settle to the Standard Model vacuum with broken $SU(5)$ symmetry, and it would be interesting to investigate whether such trajectories are compatible with the primordial black hole production. We plan to examine such questions in the future.

[1] Y. B. Zel'dovich and I. D. Novikov, The hypothesis of cores retarded during expansion and the hot cosmological model, Sov. Astron. AJ (Engl. Transl.) **10**, 602 (1967).

[2] S. Hawking, Gravitationally collapsed objects of very low mass, Mon. Not. R. Astron. Soc. **152**, 75 (1971).

[3] B. J. Carr and S. W. Hawking, Black holes in the early Universe, Mon. Not. R. Astron. Soc. **168**, 399 (1974).

[4] A. G. Polnarev and M. Y. Khlopov, Cosmology, primordial black holes, and supermassive particles, Sov. Phys. Usp. **28**, 213 (1985).

[5] B. P. Abbott *et al.* (LIGO Scientific and Virgo Collaborations), Observation of Gravitational Waves from a Binary Black Hole Merger, Phys. Rev. Lett. **116**, 061102 (2016).

[6] B. P. Abbott *et al.* (LIGO Scientific and Virgo Collaborations), GW151226: Observation of Gravitational Waves from a 22-Solar-Mass Binary Black Hole Coalescence, Phys. Rev. Lett. **116**, 241103 (2016).

[7] B. P. Abbott *et al.* (LIGO Scientific and Virgo Collaborations), GW170814: A Three-Detector Observation of Gravitational Waves from a Binary Black Hole Coalescence, Phys. Rev. Lett. **119**, 141101 (2017).

[8] B. Carr and F. Kuhnel, Primordial black holes as dark matter: Recent developments, Annu. Rev. Nucl. Part. Sci. **70**, 355 (2020).

[9] M. Y. Khlopov, Primordial black holes, Res. Astron. Astrophys. **10**, 495 (2010).

[10] M. Sasaki, T. Suyama, T. Tanaka, and S. Yokoyama, Primordial black holes—Perspectives in gravitational wave astronomy, Classical Quantum Gravity **35**, 063001 (2018).

[11] B. Carr, K. Kohri, Y. Sendouda, and J. Yokoyama, Constraints on primordial black holes, Rep. Prog. Phys. **84**, 116902 (2021).

[12] A. M. Green and B. J. Kavanagh, Primordial black holes as a dark matter candidate, J. Phys. G **48**, 043001 (2021).

[13] P. Villanueva-Domingo, O. Mena, and S. Palomares-Ruiz, A brief review on primordial black holes as dark matter, Front. Astron. Space Sci. **8**, 87 (2021).

[14] M. Sasaki, T. Suyama, T. Tanaka, and S. Yokoyama, Primordial Black Hole Scenario for the Gravitational-Wave Event GW150914, Phys. Rev. Lett. **117**, 061101 (2016); **121**, 059901(E) (2018).

[15] P. Montero-Camacho, X. Fang, G. Vasquez, M. Silva, and C. M. Hirata, Revisiting constraints on asteroid-mass primordial black holes as dark matter candidates, J. Cosmol. Astropart. Phys. 08 (2019) 031.

[16] S. Matarrese, S. Mollerach, and M. Bruni, Second order perturbations of the Einstein-de Sitter universe, Phys. Rev. D **58**, 043504 (1998).

[17] S. Mollerach, D. Harari, and S. Matarrese, CMB polarization from secondary vector and tensor modes, Phys. Rev. D **69**, 063002 (2004).

[18] K. N. Ananda, C. Clarkson, and D. Wands, The cosmological gravitational wave background from primordial density perturbations, Phys. Rev. D **75**, 123518 (2007).

[19] D. Baumann, P. J. Steinhardt, K. Takahashi, and K. Ichiki, Gravitational wave spectrum induced by primordial scalar perturbations, Phys. Rev. D **76**, 084019 (2007).

[20] J. O. Gong, Analytic integral solutions for induced gravitational waves, Astrophys. J. **925**, 102 (2022).

[21] C. Yuan and Q. G. Huang, A topic review on probing primordial black hole dark matter with scalar induced gravitational waves, arXiv:2103.04739.

[22] G. Domènech, Scalar induced gravitational waves review, Universe **7**, 398 (2021).

[23] G. Domènech, Induced gravitational waves in a general cosmological background, Int. J. Mod. Phys. D **29**, 2050028 (2020).

[24] G. Domènech, S. Pi, and M. Sasaki, Induced gravitational waves as a probe of thermal history of the universe, J. Cosmol. Astropart. Phys. 08 (2020) 017.

[25] S. Kawai and J. Kim, Primordial black holes from Gauss-Bonnet-corrected single field inflation, Phys. Rev. D **104**, 083545 (2021).

[26] S. Kawai and J. Kim, CMB from a Gauss-Bonnet-induced de Sitter fixed point, Phys. Rev. D **104**, 043525 (2021).

[27] J. Silk and M. S. Turner, Double inflation, Phys. Rev. D **35**, 419 (1987).

[28] J. Yokoyama, Formation of MACHO primordial black holes in inflationary cosmology, Astron. Astrophys. **318**, 673 (1997).

[29] L. Randall, M. Soljacic, and A. H. Guth, Supernatural inflation: Inflation from supersymmetry with no (very) small parameters, Nucl. Phys. **B472**, 377 (1996).

[30] J. Garcia-Bellido, A. D. Linde, and D. Wands, Density perturbations and black hole formation in hybrid inflation, Phys. Rev. D **54**, 6040 (1996).

[31] M. Kawasaki, N. Sugiyama, and T. Yanagida, Primordial black hole formation in a double inflation model in supergravity, Phys. Rev. D **57**, 6050 (1998).

[32] M. Kawasaki, N. Kitajima, and T. T. Yanagida, Primordial black hole formation from an axionlike curvaton model, Phys. Rev. D **87**, 063519 (2013).

[33] K. Kohri, C. M. Lin, and T. Matsuda, Primordial black holes from the inflating curvaton, Phys. Rev. D **87,** 103527 (2013).

[34] S. Clesse and J. García-Bellido, Massive primordial black holes from hybrid inflation as dark matter and the seeds of Galaxies, Phys. Rev. D **92,** 023524 (2015).

[35] K. Ando, K. Inomata, M. Kawasaki, K. Mukaida, and T. T. Yanagida, Primordial black holes for the LIGO events in the axionlike curvaton model, Phys. Rev. D **97,** 123512 (2018).

[36] S. Pi, Y. L. Zhang, Q. G. Huang, and M. Sasaki, Scalaron from R^2-gravity as a heavy field, J. Cosmol. Astropart. Phys. 05 (2018) 042.

[37] D. Y. Cheong, S. M. Lee, and S. C. Park, Primordial black holes in Higgs-R^2 inflation as the whole of dark matter, J. Cosmol. Astropart. Phys. 01 (2021) 032.

[38] S. V. Ketov and M. Y. Khlopov, Cosmological probes of supersymmetric field theory models at superhigh energy scales, Symmetry **11,** 511 (2019).

[39] A. Ashoorioon, A. Rostami, and J. T. Firouzjaee, Examining the end of inflation with primordial black holes mass distribution and gravitational waves, Phys. Rev. D **103,** 123512 (2021).

[40] A. Gundhi, S. V. Ketov, and C. F. Steinwachs, Primordial black hole dark matter in dilaton-extended two-field Starobinsky inflation, Phys. Rev. D **103,** 083518 (2021).

[41] A. Gundhi and C. F. Steinwachs, Scalaron–Higgs inflation reloaded: Higgs-dependent scalaron mass and primordial black hole dark matter, Eur. Phys. J. C **81,** 460 (2021).

[42] G. A. Palma, S. Sypsas, and C. Zenteno, Seeding Primordial Black Holes in Multifield Inflation, Phys. Rev. Lett. **125,** 121301 (2020).

[43] M. Braglia, X. Chen, and D. K. Hazra, Probing primordial features with the stochastic gravitational wave background, J. Cosmol. Astropart. Phys. 03 (2021) 005.

[44] M. Braglia, D. K. Hazra, F. Finelli, G. F. Smoot, L. Sriramkumar, and A. A. Starobinsky, Generating PBHs and small-scale GWs in two-field models of inflation, J. Cosmol. Astropart. Phys. 08 (2020) 001.

[45] Y. Aldabergenov, A. Addazi, and S. V. Ketov, Primordial black holes from modified supergravity, Eur. Phys. J. C **80,** 917 (2020).

[46] V. C. Spanos and I. D. Stamou, Gravitational waves and primordial black holes from supersymmetric hybrid inflation, Phys. Rev. D **104,** 123537 (2021).

[47] S. V. Ketov, Multi-field versus single-field in the supergravity models of inflation and primordial black holes, Universe **7,** 115 (2021).

[48] L. Iacconi, H. Assadullahi, M. Fasiello, and D. Wands, Revisiting small-scale fluctuations in α-attractor models of inflation, J. Cosmol. Astropart. Phys. 06 (2022) 007.

[49] S. Hooshangi, A. Talebian, M. H. Namjoo, and H. Firouzjahi, Multiple field ultraslow-roll inflation: Primordial black holes from straight bulk and distorted boundary, Phys. Rev. D **105,** 083525 (2022).

[50] A. Ashoorioon, K. Rezazadeh, and A. Rostami, NANO-Grav Signal from the end of inflation and the LIGO mass and heavier primordial black holes, Phys. Lett. B **835,** 137542 (2022).

[51] K. Boutivas, I. Dalianis, G. P. Kodaxis, and N. Tetradis, The effect of multiple features on the power spectrum in two-field inflation, J. Cosmol. Astropart. Phys. 08 (2022) 021.

[52] D. Y. Cheong, K. Kohri, and S. C. Park, The inflaton that could: Primordial black holes and second order gravitational waves from tachyonic instability induced in Higgs-R^2 inflation, J. Cosmol. Astropart. Phys. 10 (2022) 015.

[53] S. Geller, W. Qin, E. McDonough, and D. I. Kaiser, Primordial black holes from multifield inflation with nonminimal couplings, Phys. Rev. D **106,** 063535 (2022).

[54] S. Bhattacharya and I. Zavala, Sharp turns in axion monodromy: Primordial black holes and gravitational waves, arXiv:2205.06065.

[55] J. L. Cervantes-Cota and H. Dehnen, Induced gravity inflation in the standard model of particle physics, Nucl. Phys. **B442,** 391 (1995).

[56] F. L. Bezrukov and M. Shaposhnikov, The Standard Model Higgs boson as the inflaton, Phys. Lett. B **659,** 703 (2008).

[57] M. B. Einhorn and D. R. T. Jones, Inflation with non-minimal gravitational couplings in supergravity, J. High Energy Phys. 03 (2010) 026.

[58] S. Ferrara, R. Kallosh, A. Linde, A. Marrani, and A. Van Proeyen, Superconformal symmetry, NMSSM, and inflation, Phys. Rev. D **83,** 025008 (2011).

[59] S. Ferrara, R. Kallosh, A. Linde, A. Marrani, and A. Van Proeyen, Jordan frame supergravity and inflation in NMSSM, Phys. Rev. D **82,** 045003 (2010).

[60] M. Arai, S. Kawai, and N. Okada, Higgs inflation in minimal supersymmetric SU(5) GUT, Phys. Rev. D **84,** 123515 (2011).

[61] S. Kawai and J. Kim, Multifield dynamics of supersymmetric Higgs inflation in SU(5) GUT, Phys. Rev. D **93,** 065023 (2016).

[62] C. Pallis and N. Toumbas, Non-minimal Higgs inflation and non-thermal leptogenesis in a supersymmetric Pati-Salam model, J. Cosmol. Astropart. Phys. 12 (2011) 002.

[63] M. Arai, S. Kawai, and N. Okada, Supersymmetric Standard Model inflation in the planck era, Phys. Rev. D **86,** 063507 (2012).

[64] M. Arai, S. Kawai, and N. Okada, Higgs-lepton inflation in the supersymmetric minimal seesaw model, Phys. Rev. D **87,** 065009 (2013).

[65] S. Kawai and N. Okada, TeV scale Seesaw from super-symmetric Higgs-lepton inflation and BICEP2, Phys. Lett. B **735,** 186 (2014).

[66] S. Kawai and J. Kim, Testing supersymmetric Higgs inflation with non-Gaussianity, Phys. Rev. D **91,** 045021 (2015).

[67] S. Kawai and N. Okada, Inflation and type III seesaw mechanism in ν-gauge mediated supersymmetry breaking, Phys. Rev. D **104,** 115031 (2021).

[68] M. Arai, S. Kawai, and N. Okada, Supersymmetric $B - L$ inflation near the conformal coupling, Phys. Lett. B **734,** 100 (2014).

[69] G. K. Leontaris, N. Okada, and Q. Shafi, Non-minimal quartic inflation in supersymmetric $SO(10)$, Phys. Lett. B **765,** 256 (2017).

[70] N. Okada and Q. Shafi, Gravity waves and gravitino dark matter in μ-hybrid inflation, Phys. Lett. B **787,** 141 (2018).

[71] S. Kawai and N. Okada, Messenger inflation in gauge mediation and super-WIMP dark matter, Phys. Rev. D **104,** 083539 (2021).

[72] S. Kawai and N. Okada, Gravitino constraints on supergravity inflation, Phys. Rev. D **105,** L101302 (2022).

[73] C. M. Peterson and M. Tegmark, Testing two-field inflation, Phys. Rev. D **83,** 023522 (2011).

[74] M. Sasaki and E. D. Stewart, A general analytic formula for the spectral index of the density perturbations produced during inflation, Prog. Theor. Phys. **95,** 71 (1996).

[75] T. T. Nakamura and E. D. Stewart, The spectrum of cosmological perturbations produced by a multicomponent inflaton to second order in the slow roll approximation, Phys. Lett. B **381,** 413 (1996).

[76] C. Gordon, D. Wands, B. A. Bassett, and R. Maartens, Adiabatic and entropy perturbations from inflation, Phys. Rev. D **63,** 023506 (2000).

[77] S. Groot Nibbelink and B. J. W. van Tent, Scalar perturbations during multiple field slow-roll inflation, Classical Quantum Gravity **19,** 613 (2002).

[78] J. O. Gong and T. Tanaka, A covariant approach to general field space metric in multi-field inflation, J. Cosmol. Astropart. Phys. 03 (2011) 015; 02 (2012) E01.

[79] D. I. Kaiser, E. A. Mazenc, and E. I. Sfakianakis, Primordial bispectrum from multifield inflation with nonminimal couplings, Phys. Rev. D **87,** 064004 (2013).

[80] K. Schutz, E. I. Sfakianakis, and D. I. Kaiser, Multifield inflation after Planck: Isocurvature modes from nonminimal couplings, Phys. Rev. D **89,** 064044 (2014).

[81] Y. Akrami *et al.* (Planck Collaboration), Planck 2018 results. X. Constraints on inflation, Astron. Astrophys. **641,** A10 (2020).

[82] P. A. R. Ade *et al.* (BICEP and Keck Collaborations), Improved Constraints on Primordial Gravitational Waves using Planck, WMAP, and BICEP/Keck Observations through the 2018 Observing Season, Phys. Rev. Lett. **127,** 151301 (2021).

[83] M. Dias, J. Frazer, and D. Seery, Computing observables in curved multifield models of inflation—A guide (with code) to the transport method, J. Cosmol. Astropart. Phys. 12 (2015) 030.

[84] M. Dias, J. Frazer, D. J. Mulryne, and D. Seery, Numerical evaluation of the bispectrum in multiple field inflation—The transport approach with code, J. Cosmol. Astropart. Phys. 12 (2016) 033.

[85] D. Seery, CppTransport: A platform to automate calculation of inflationary correlation functions, arXiv:1609.00380.

[86] D. J. Mulryne and J. W. Ronayne, PyTransport: A PYTHON package for the calculation of inflationary correlation functions, J. Open Source Softwaare **3,** 494 (2018).

[87] J. W. Ronayne and D. J. Mulryne, Numerically evaluating the bispectrum in curved field-space—with PyTransport 2.0, J. Cosmol. Astropart. Phys. 01 (2018) 023.

[88] R. Rosati, Inflation.jl—A Julia package for numerical evaluation of cosmic inflation models using the transport method, Juliacon 2020, Zenodo, 10.5281/zenodo.4708348 (2020).

[89] D. J. Mulryne, D. Seery, and D. Wesley, Moment transport equations for non-Gaussianity, J. Cosmol. Astropart. Phys. 01 (2010) 024.

[90] D. J. Mulryne, D. Seery, and D. Wesley, Moment transport equations for the primordial curvature perturbation, J. Cosmol. Astropart. Phys. 04 (2011) 030.

[91] M. Dias and D. Seery, Transport equations for the inflationary spectral index, Phys. Rev. D **85,** 043519 (2012).

[92] G. J. Anderson, D. J. Mulryne, and D. Seery, Transport equations for the inflationary trispectrum, J. Cosmol. Astropart. Phys. 10 (2012) 019.

[93] J. Elliston, D. Seery, and R. Tavakol, The inflationary bispectrum with curved field-space, J. Cosmol. Astropart. Phys. 11 (2012) 060.

[94] D. J. Mulryne, Transporting non-Gaussianity from sub to super-horizon scales, J. Cosmol. Astropart. Phys. 09 (2013) 010.

[95] M. Dias, J. Elliston, J. Frazer, D. Mulryne, and D. Seery, The curvature perturbation at second order, J. Cosmol. Astropart. Phys. 02 (2015) 040.

[96] B. J. Carr, The Primordial black hole mass spectrum, Astrophys. J. **201,** 1 (1975).

[97] A. S. Josan, A. M. Green, and K. A. Malik, Generalised constraints on the curvature perturbation from primordial black holes, Phys. Rev. D **79,** 103520 (2009).

[98] S. Young, C. T. Byrnes, and M. Sasaki, Calculating the mass fraction of primordial black holes, J. Cosmol. Astropart. Phys. 07 (2014) 045.

[99] J. S. Bullock and J. R. Primack, Non-Gaussian fluctuations and primordial black holes from inflation, Phys. Rev. D **55,** 7423 (1997).

[100] P. Ivanov, Nonlinear metric perturbations and production of primordial black holes, Phys. Rev. D **57,** 7145 (1998).

[101] D. H. Lyth, The hybrid inflation waterfall and the primordial curvature perturbation, J. Cosmol. Astropart. Phys. 05 (2012) 022.

[102] C. T. Byrnes, E. J. Copeland, and A. M. Green, Primordial black holes as a tool for constraining non-Gaussianity, Phys. Rev. D **86,** 043512 (2012).

[103] E. V. Bugaev and P. A. Klimai, Primordial black hole constraints for curvaton models with predicted large non-Gaussianity, Int. J. Mod. Phys. D **22,** 1350034 (2013).

[104] S. Young and C. T. Byrnes, Primordial black holes in non-Gaussian regimes, J. Cosmol. Astropart. Phys. 08 (2013) 052.

[105] T. Nakama, J. Silk, and M. Kamionkowski, Stochastic gravitational waves associated with the formation of primordial black holes, Phys. Rev. D **95,** 043511 (2017).

[106] J. Garcia-Bellido, M. Peloso, and C. Unal, Gravitational wave signatures of inflationary models from primordial black hole dark matter, J. Cosmol. Astropart. Phys. 09 (2017) 013.

[107] G. Franciolini, A. Kehagias, S. Matarrese, and A. Riotto, Primordial black holes from inflation and non-Gaussianity, J. Cosmol. Astropart. Phys. 03 (2018) 016.

[108] R. G. Cai, S. Pi, and M. Sasaki, Gravitational Waves Induced by Non-Gaussian Scalar Perturbations, Phys. Rev. Lett. **122,** 201101 (2019).

[109] V. Atal and C. Germani, The role of non-Gaussianities in primordial black hole formation, Phys. Dark Universe **24,** 100275 (2019).

[110] C. Unal, Imprints of primordial non-Gaussianity on gravitational wave spectrum, Phys. Rev. D **99,** 041301 (2019).

[111] S. Passaglia, W. Hu, and H. Motohashi, Primordial black holes and local non-Gaussianity in canonical inflation, Phys. Rev. D **99,** 043536 (2019).

[112] V. Atal, J. Garriga, and A. Marcos-Caballero, Primordial black hole formation with non-Gaussian curvature perturbations, J. Cosmol. Astropart. Phys. 09 (2019) 073.

[113] G. Panagopoulos and E. Silverstein, Primordial black holes from non-Gaussian tails, arXiv:1906.02827.

[114] C. M. Yoo, J. O. Gong, and S. Yokoyama, Abundance of primordial black holes with local non-Gaussianity in peak theory, J. Cosmol. Astropart. Phys. 09 (2019) 033.

[115] A. Kehagias, I. Musco, and A. Riotto, Non-Gaussian formation of primordial black holes: Effects on the threshold, J. Cosmol. Astropart. Phys. 12 (2019) 029.

[116] J. M. Ezquiaga, J. García-Bellido, and V. Vennin, The exponential tail of inflationary fluctuations: Consequences for primordial black holes, J. Cosmol. Astropart. Phys. 03 (2020) 029.

[117] C. Yuan and Q. G. Huang, Gravitational waves induced by the local-type non-Gaussian curvature perturbations, Phys. Lett. B **821,** 136606 (2021).

[118] H. V. Ragavendra, P. Saha, L. Sriramkumar, and J. Silk, Primordial black holes and secondary gravitational waves from ultraslow roll and punctuated inflation, Phys. Rev. D **103,** 083510 (2021).

[119] P. Adshead, K. D. Lozanov, and Z. J. Weiner, Non-Gaussianity and the induced gravitational wave background, J. Cosmol. Astropart. Phys. 10 (2021) 080.

[120] V. Atal and G. Domènech, Probing non-Gaussianities with the high frequency tail of induced gravitational waves, J. Cosmol. Astropart. Phys. 06 (2021) 001.

[121] B. J. Kavanagh, bradkav/PBHbounds: Release version (1.0), Zenodo, 10.5281/zenodo.3538999 (2019).

[122] R. Laha, Primordial Black Holes as a Dark Matter Candidate are Severely Constrained by the Galactic Center 511 keV γ-Ray Line, Phys. Rev. Lett. **123,** 251101 (2019).

[123] R. Laha, J. B. Muñoz, and T. R. Slatyer, INTEGRAL constraints on primordial black holes and particle dark matter, Phys. Rev. D **101,** 123514 (2020).

[124] A. K. Saha and R. Laha, Sensitivities on nonspinning and spinning primordial black hole dark matter with global 21-cm troughs, Phys. Rev. D **105,** 103026 (2022).

[125] A. Ray, R. Laha, J. B. Muñoz, and R. Caputo, Near future MeV telescopes can discover asteroid-mass primordial black hole dark matter, Phys. Rev. D **104,** 023516 (2021).

[126] M. Maggiore, Gravitational wave experiments and early universe cosmology, Phys. Rep. **331,** 283 (2000).

[127] M. Maggiore, *Gravitational Waves. Vol. 1: Theory and Experiments* (Oxford University Press, New York, 2007), ISBN 978-0-19-857074-5, 978-0-19-852074-0.

[128] K. Kohri and T. Terada, Semianalytic calculation of gravitational wave spectrum nonlinearly induced from primordial curvature perturbations, Phys. Rev. D **97,** 123532 (2018).

[129] K. Inomata, M. Kawasaki, K. Mukaida, Y. Tada, and T. T. Yanagida, Inflationary primordial black holes for the LIGO gravitational wave events and pulsar timing array experiments, Phys. Rev. D **95,** 123510 (2017).

[130] K. Ando, K. Inomata, and M. Kawasaki, Primordial black holes and uncertainties in the choice of the window function, Phys. Rev. D **97,** 103528 (2018).

[131] P. Amaro-Seoane *et al.* (LISA Collaboration), Laser interferometer space antenna, arXiv:1702.00786.

[132] J. Baker, J. Bellovary, P. L. Bender, E. Berti, R. Caldwell, J. Camp, J. W. Conklin, N. Cornish, C. Cutler, R. DeRosa *et al.*, The laser interferometer space antenna: Unveiling the millihertz gravitational wave sky, arXiv:1907.06482.

[133] N. Seto, S. Kawamura, and T. Nakamura, Possibility of Direct Measurement of the Acceleration of the Universe Using 0.1-Hz Band Laser Interferometer Gravitational Wave Antenna in Space, Phys. Rev. Lett. **87,** 221103 (2001).

[134] S. Kawamura, T. Nakamura, M. Ando, N. Seto, K. Tsubono, K. Numata, R. Takahashi, S. Nagano, T. Ishikawa, M. Musha *et al.*, The Japanese space gravitational wave antenna DECIGO, Classical Quantum Gravity **23,** S125 (2006).

[135] S. Sato, S. Kawamura, M. Ando, T. Nakamura, K. Tsubono, A. Araya, I. Funaki, K. Ioka, N. Kanda, S. Moriwaki *et al.*, The status of DECIGO, J. Phys. Conf. Ser. **840,** 012010 (2017).

[136] S. Isoyama, H. Nakano, and T. Nakamura, Multiband gravitational-wave astronomy: Observing binary inspirals with a decihertz detector, B-DECIGO, Prog. Theor. Exp. Phys. **2018,** 073E01 (2018).

[137] S. Kawamura, M. Ando, N. Seto, S. Sato, M. Musha, I. Kawano, J. Yokoyama, T. Tanaka, K. Ioka, and T. Akutsu *et al.*, Current status of space gravitational wave antenna DECIGO and B-DECIGO, Prog. Theor. Exp. Phys. **2021,** 05A105 (2021).

[138] V. Corbin and N. J. Cornish, Detecting the cosmic gravitational wave background with the big bang observer, Classical Quantum Gravity **23,** 2435 (2006).

[139] J. Crowder and N. J. Cornish, Beyond LISA: Exploring future gravitational wave missions, Phys. Rev. D **72,** 083005 (2005).

[140] G. M. Harry, P. Fritschel, D. A. Shaddock, W. Folkner, and E. S. Phinney, Laser interferometry for the big bang observer, Classical Quantum Gravity **23,** 4887 (2006); **23,** 7361(E) (2006).

[141] C. L. Carilli and S. Rawlings, Science with the square kilometer array: Motivation, key science projects, standards and assumptions, New Astron. Rev. **48,** 979 (2004).

[142] G. Janssen, G. Hobbs, M. McLaughlin, C. Bassa, A. T. Deller, M. Kramer, K. Lee, C. Mingarelli, P. Rosado, and S. Sanidas *et al.*, Gravitational wave astronomy with the SKA, Proc. Sci. AASKA14 (**2015**) 037.

[143] A. Weltman, P. Bull, S. Camera, K. Kelley, H. Padmanabhan, J. Pritchard, A. Raccanelli, S. Riemer-Sørensen, L. Shao, and S. Andrianomena *et al.*, Fundamental physics with the square kilometre array, Pub. Astron. Soc. Aust. **37,** e002 (2020).

[144] K. Schmitz, New sensitivity curves for gravitational-wave signals from cosmological phase transitions, J. High Energy Phys. 01 (2021) 097.

[145] K. Schmitz, New sensitivity curves for gravitational-wave experiments, Zenodo, 10.5281/zenodo.3689582 (2020).